Available online at www.sciencedirect.com
SCIENCE DIRECT®
Journal of Solid State Chemistry 177 (2004) 4605–4615
JOURNAL OF SOLID STATE CHEMISTRY
www.elsevier.com/locate/jssc

Octahedral distortions in the homometallic Fe ludwigite

Maria Matos*

Departamento de Física, Pontificia Universidade Catolica do Rio de Janeiro, CEP: 22453-970 Rio de Janeiro, Caixa Postal 38071, Gávea, Brazil

Received 6 August 2004; received in revised form 8 October 2004; accepted 10 October 2004
Available online 11 November 2004

Abstract

An extended Hückel *high spin band* approach is used to investigate the effects of oxygen octahedral distortions in the $Fe_3O_2BO_3$ ludwigite. Owing to distortion, a 0.2 eV stabilizing gap (above the *spin down* Fermi level) is found to appear in a 1D sub-unit, formed by the strongly interacting Fe^{3+}–Fe^{2+}–Fe^{3+} triad. Through a detailed analysis of the crystal wave functions, the gap is found to be a result of $3d(\sigma)$–$3d(\pi)$ orbital mixing, which generates a narrow band for the extra (spin down) Fe^{2+} electron. Charge localization is obtained in the 1D sub-unit but not in the whole crystal (3D) calculation. It is suggested that the high barrier for electron hopping, experimentally found in the literature to occur around 220 K, be related to the 1D gap.

Keywords: Ludwigite; $Fe_3O_2BO_3$; Oxyborate; Electronic structure; Extended Hückel; Distortion; Octahedral field; Charge distribution; High spin band; Band structure analysis

1. Introduction

The homometallic iron ludwigite $Fe_3O_2BO_3$ has been the subject of continuous research in the last few years due to a variety of interesting physical properties exhibited by this material [1–6]. It is a compound of mixed valence with one trivalent and two divalent cations per formula unit, with metallic ions most probably in the high spin states $S=5/2$ and $S=2$. Experimental data on magnetic properties indicate antiferromagnetic behavior below 112 K and weak ferromagnetism in the range 70–40 K [2]. Below 40 K the material is again antiferromagnetic. The suggestion that two spin sublattices coexist in the iron ludwigite has been supported by a recent theoretical work [5].

Transport measurements in $Fe_3O_2BO_3$ [2] have shown that the electrical resistivity is high at temperatures below 220 K, showing activated behavior with small (a few meV) characteristic energy. Above 220 K, the resistivity decreases considerably and, at the same time, the characteristic energy raises to about 0.1 eV. The cross over temperature (220 K) has been associated with charge localization in the material, a process that was also predicted by Swinnea et al. [1].

The ludwigites, of general formula $M_2M'O_2BO_3$, where $M(M')$ is a di(tri)valent cation, have a crystalline structure formed by corrugated planes of metal-containing oxygen octahedra pilling up along the *c*-axis of a flat orthorhombic unit cell—*c* is about 3 times shorter than the other unit cell parameters a and b. The structure is similar to another oxyborate, the warwickite, formed by one-dimensional stripes instead of walls [7]. Strongly covalent BO_3 sub-units hold the zigzag planes together [8]. In Fig. 1, the crystalline structure of $Fe_3O_2BO_3$ is seen in a view along the *c*-axis. There are four formula units in the unit cell and the 12 Fe atoms are arranged in four non-equivalent octahedral sites (1–4). Empirical estimates based on bond valence sums predict that sites 1 and 3 are occupied by divalent ions, with site 4 being preferentially occupied by the trivalent ion [5,7]. Mössbauer spectroscopy shows evidence of valences +2, +3 and +2.5, having been suggested that Fe(2) and Fe(4) share the intermediate valence [1,2]. The triad of atoms Fe(4)–Fe(2)–Fe(4) constitutes an important group in the compound due to the short Fe–Fe distance

*Fax: +55 21 3114 1271.
E-mail address: mmatos@fis.puc-rio.br (M. Matos).

0022-4596/$ - see front matter © 2004 Elsevier Inc. All rights reserved.
doi:10.1016/j.jssc.2004.10.018

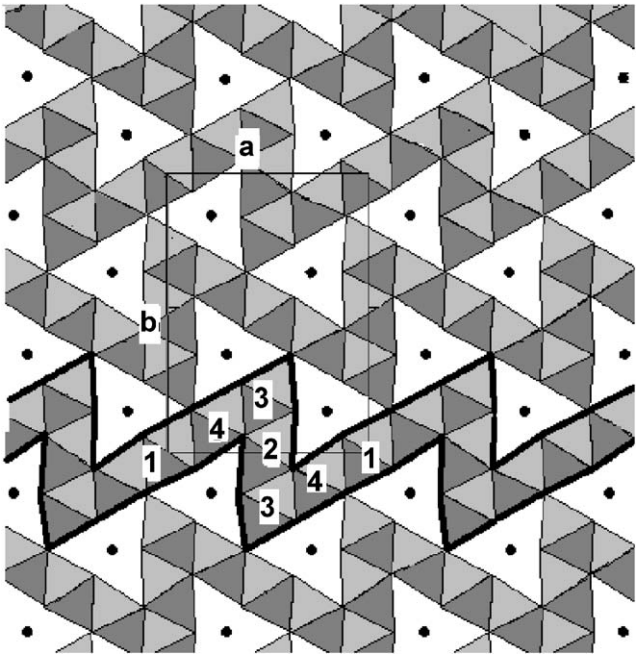

Fig. 1. The polyhedral representation of the ludwigite crystalline structure, seen in a projection parallel to the ab plane; the four distinct crystallographic sites, 1–4, are indicated. Boron atoms are represented by small black dots. BO_3 units are formed with the three O atoms located in the vertices of nearest neighbor octahedra, in the middle of the edges of the B centered empty triangles.

(2.787 Å) of its next neighbor pairs. It is responsible for the anti-ferromagnetic transition at 112 K, which couples spins along *c*, in a one-dimensional pattern [2,5]. More recently [6] it was found that the homometallic Fe ludwigite undergoes a structural phase transition at 283 K in which the size of the unit cell is doubled along *c*. In the less symmetric low-temperature crystal phase, the two Fe(4) atoms are no longer eqüidistant from Fe(2), forming a geometrical arrangement in which shorter and larger Fe(2)–Fe(4) distances alternate as one moves along *c*, giving rise to unit cell duplication.

Metal borates have stimulated a number of theoretical papers. Recently [9], the pseudopotential method was used to study the origin of optical anisotropy in $BaB_5O_8(OH)_3$. A different approach was used in $Fe_3O_2BO_3$ in which the tight binding Hamiltonian was used to analyze the effects of Fe–Fe interactions in the charge distribution at the different metal sites [4]. Also, Whangbo et al. [5] investigated spin exchange interactions in $Fe_3O_2BO_3$ by considering different spin dimers (a pair of Fe containing oxygen octahedra sharing edges or vertices) in the material's structure. In that paper, a complete explanation of the magnetic behavior of $Fe_3O_2BO_3$ was provided. The strongest exchange path was found to connect two Fe(4) ($S=5/2$) spins in the *c*-axis direction, in accordance with the 1D AF transition at 112 K. A weaker exchange path connects Fe(1) and Fe(3) ($S=2$) spins in different walls, thus explaining why the AF arrangement involving the whole crystal occurs at a much lower temperature (40 K). The calculations confirm the existence of two independent spin systems in the material.

From these results, the importance of octahedral geometry in explaining the physical properties of the compound could be inferred: magnetic properties, as seen, are intrinsically connected to molecular states in the several Fe–O dimers found in the structure of $Fe_3O_2BO_3$. If the octahedral geometry is essential to explain magnetism, it could be expected to affect other electronic properties of the system. A study on the effects of oxygen distortions on extended properties of the ludwigite has not been carried out until very recently. This is the aim of the present paper. Since the structural transition does not lead to essential modifications in the compound's electronic structure, the present study is based on the structurally simpler high-temperature (294 K) phase. The theoretical analysis is based on the *high spin band* approach within the tight binding-with overlap extended Hückel theory. The approach could be seen as the extended structure analogue of that developed by Whangbo et al. [5].

2. Method

The extended Hückel theory (eHT) is well known in the literature [10–13]. The empirical parameters used in all the calculations of the present paper were obtained from standard eHT tables, whose values for the diagonal Hamiltonian matrix elements H_{ii} and Slater Atomic Orbitals exponents ζ are the following: (a) for *B*, $H_{2s,2s}=-15.2$ eV with $\zeta_{2s}=1.3$, $H_{2p,2p}=-8.5$ eV with $\zeta_{2p}=1.3$, (b) for *O*, $H_{2s,2s}=-32.3$ eV with $\zeta_{2s}=2.275$, $H_{2p,2p}=-14.8$ eV with $\zeta_{2p}=2.275$ and (c) For Fe, $H_{4s,4s}=-9.10$ eV with $\zeta_{4s}=1.9$, $H_{4p,4p}=-5.32$ eV with $\zeta_{4p}=1.9$, $H_{3d,3d}=-12.6$ eV with $\zeta_1=5.35$ and $\zeta_2=2.0$ in a linear double zeta combination with coefficients $c_1=0.5505$ and $c_2=0.6260$, respectively.

DOS and COOP [13] calculations for the 3D crystal will be performed with a set of 192 K points, built in such a way as to fill the orthorhombic first Brillouin zone with a uniform density of points. In the 1D subunits, calculations were performed with a set of 125 k points.

3. Crystal structure and 1D models

The crystalline structure of $Fe_3O_2BO_3$ at 294 K was recently determined from X-ray difraction data [2,6], reproducing earlier structural data [1] with minor differences in the crystal lattice parameters. The crystal space group is found to be *Pbam*, more symmetric than

that obtained at 144 K (*Pbnm*) [6]. Some structural data of the *Pbam* phase, important to this study, are summarized in Table 1. Note first that lattice parameters *a* and *b* are significantly greater than *c*, thus explaining why band dispersion along those directions is small [4]. Fe–Fe distance corresponding to octahedra sharing edges along *c* (3.073 Å) is smaller than other Fe–Fe distances, with the exception of Fe(2)–Fe(4). The smallest octahedron is that related to site 4, as seen from the average Fe–O distance, with sites 1 and 3 providing the two biggest ones. These octahedral sizes are consistent with bond valences, calculated from the empirical formula of Brown and Altermatt [14], of 2.67, 2.02 and 2.04, respectively, for sites 4, 1 and 3, clearly suggesting valences 3^+ (for site 4) and 2^+ (for 1 and 3), as pointed out in [5]. Note that smaller Fe–O distances provide stronger 3*d* electron repulsion, thus leading to increasing oxidation state. Site 2 corresponds to an average size octahedron, with valence 2.28, if one uses Fe^{2+} parameters. Fe^{3+} parameters give rise to a valence of 2.44, not very different from 2.28 [5], indicative of intermediate valence.

Table 1
Crystallographic data of $Fe_3O_2BO_3$ at the 294 K phase. Distances in Å

Crystal lattice parameters			
a	*b*	*c*	
9.462	12.308	3.075	
Fe–Fe distances			
1–4	2–3	2–4	3–4
3.101	3.176	2.787	3.191
Fe–O distances			
1	2	3	4
2.199	1.952	2.102	2.074
2.199	2.017	2.206	2.091
2.199	2.186	2.206	2.091
2.199	2.186	1.955	2.007
2.037	2.017	2.208	2.007
2.037	2.171	2.208	2.069
Fe–O average distances			
1	2	3	4
2.145	2.088	2.147	2.057

In the high spin configuration of Fe^{2+} ($S=2$), distortion of the perfect octahedral ligand field is expected since it stabilizes the FeO_6 monomer, by breaking the degeneracy of the lower t_{2g} group, in the three below two *d*-separation of the octahedral field. One could use a previous analysis [4] which showed that, in fact, sites 1 and 3 (site 4 in Ref. [4]) are those in which distortion is more effective in the monomer. Therefore, octahedral distortion in $Fe_3O_2BO_3$ must play an important role given that the majority of Fe atoms are in the oxidation state $+2$ (8 in 12, per unit cell). (For clarity, the denominations t_{2g} and e_g will be used in this paper for the group of levels originating from these group theory representations when distortion is present.)

A convenient procedure to understand distortion is to compare the actual structure with an *ideal* one, similar to the former except for having perfect octahedra surrounding the metal sites. Because this is a complicate task to be done in the whole crystal, a sub-unit was chosen, formed by the 424 triad and running along the *c*-axis. Besides its simplicity and crystallographic importance (it is the most strongly Fe–Fe interacting group and holds the trivalent cations), the $(Fe_3O_{10})^{12-}$

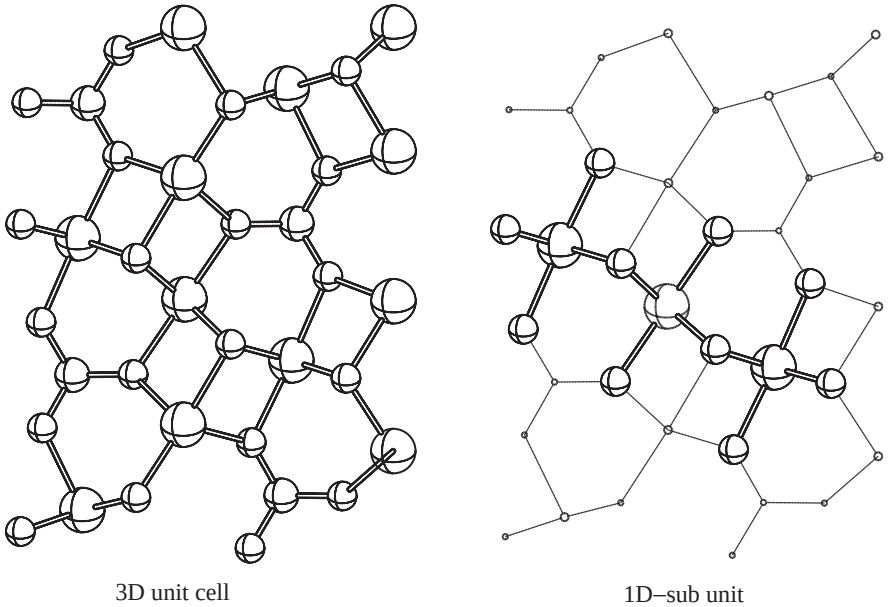

Fig. 2. The 1D sub-unit (right), containing the Fe(4)–Fe(2)–Fe(4) triad, carved out from the unit cell of $Fe_3O_2BO_3$ (left). Big spheres:Fe; medium spheres: O; small spheres: B. Fe(2) is at the center of the triad.

one-dimensional sub-unit, or ribbon, so formed, presents important physical properties, as mentioned in Section 1. In Fig. 2, the sub-unit is shown, carved out directly from the 3D crystal structure.

The ideal sub-unit was built so as to reproduce another 424 triad chain, equal to the former but with perfectly regular and identical octahedra. Their size, 2.1 Å, was taken as the average Fe–O distance of the triad (see Table 1). This choice, although reasonable, is somewhat arbitrary; it provides a convenient model for symmetry analysis purpose; results based on quantitative comparisons between actual and ideal structures must, nevertheless, be taken with care. The ideal and ludwigite ribbons are shown in Fig. 3, both drawn in a new coordinate system within which the ribbon is made to run along the x-axis. A comment should be made on the new coordinate system. In the ludwigite structure, the 424 axis does not lie along any particular coordinate axis. Detailed analysis were done in similar systems, with a coordinate system analogous to that in Fig. 3, that is, one in which the metal–metal axis lies along z [8,15]. To benefit from that analysis, the 424 triad chain has been reoriented, to get the situation shown in Fig. 3. Note that under distortion the O–Fe(2)–O axis (along the y-direction) rotates in a direction opposite to that of O–Fe(4)–O axis (these oxygen atoms will be called "axial"), causing the two edge sharing O–O axis ("bridging" oxygens) to move up and down. Such oxygen movements cause the proximity of two axial O atoms bonded to Fe(2) and Fe(4), respectively. Two axial O–O pairs are formed in the triad.

Molecular sub-units $(Fe_3O_{14})^{20-}$ (424 cluster) are also used in the study. They consist of three isolated edge-sharing Fe containing O octahedra, taken from the ludwigite structure.

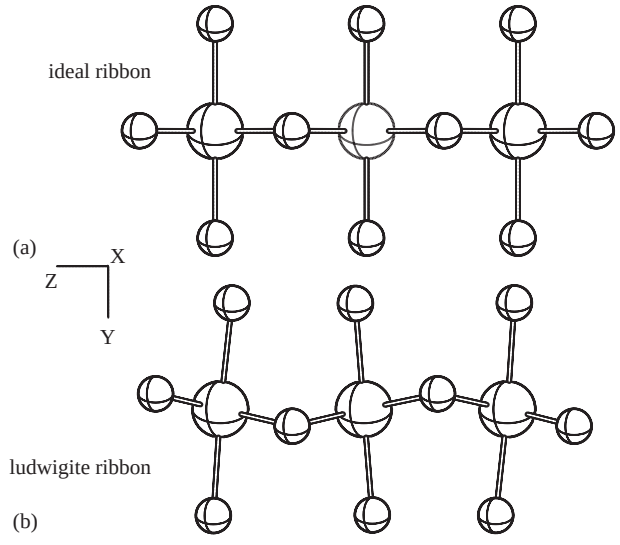

Fig. 3. The ideal (a) and ludwigite (b) ribbons sketched in a convenient coordinate system. Big spheres: Fe; medium spheres: O.

4. Results

In this section, an electronic structure analysis of the ludwigite and ideal systems is performed. It is interesting to examine first the isolated molecular sub-unit. In Fig. 4, its molecular orbital energy levels, arising from the mutual interactions of Fe 3d atomic levels, are seen in comparison with those of the ideal cluster. The lower and higher levels of the t_{2g} group, slightly set apart from the other t_{2g} levels, are mainly σ bonding and antibonding combinations of 3d orbitals (a more detailed analysis of this effect in the similar warwickite system could be found in [8]). For the ludwigite cluster (Fig. 4a), the total contribution, given by the square of the atomic orbital (AO) coefficient in the corresponding molecular orbital (MO), is 0.69(0.80) for z^2 and 0.13(0.16) for x^2-y^2, in σ (σ^*); there is also a weaker contribution of yz (respectively, 0.06 and 0.04 at σ and σ^*). For the ideal model, results are similar except for the mixing with yz, which is symmetry-forbiden in this case. As will be seen below, z^2-yz and $(x^2-y^2)-yz$ interactions play an important role in the stabilization of $Fe_3O_2BO_3$.

High spin configuration in an $Fe^{2+}O_6$ monomer is attained if the 6 Fe^{2+} electrons are distributed in such a way that 5 (spin up) electrons occupy the 5 3d-O levels,

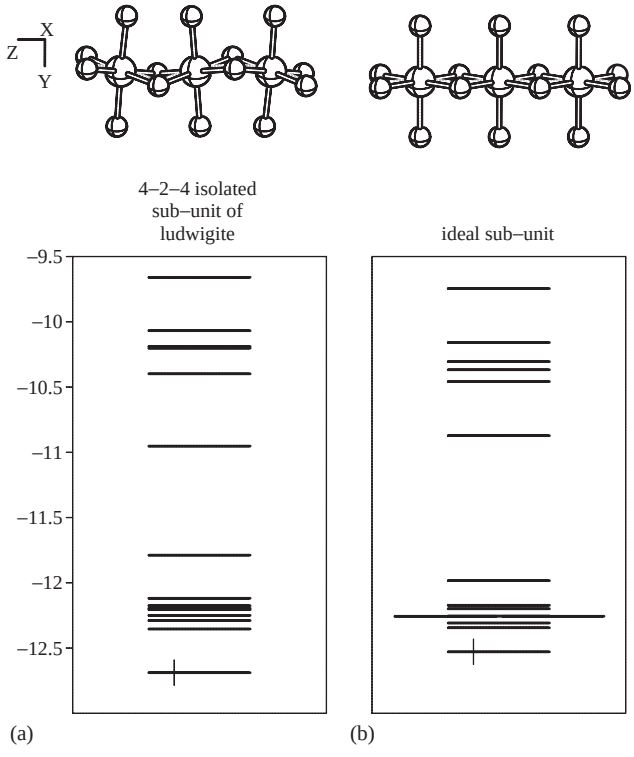

Fig. 4. Molecular orbital energies of the isolated sub-units $Fe_3O_{14}^{20-}$ in the ludwigite (a) and ideal (b) structures. The spin down HOMO is shown with the Fe^{2+} extra electron of the 424 triad. Energies in eV. The group of levels below −11.5 eV comes from the t_{2g} group of the individual FeO_6; e_g group: above −11.5 eV.

split according to the particular geometry of the octahedron, with the extra (spin down) electron filling the lower t_{2g} level. For $Fe^{3+}O_6$, there is only 5 spin up electrons, so all 3*d*–O levels are singly occupied. In the 424 cluster there are $5+5+6=16$ electrons coming from the two Fe^{3+} and one Fe^{2+} cations. From these, 15 have spin pointed up, with the extra Fe^{2+} electron pointing down. According to the extended Hückel-high spin approach [5] one thinks of the 15 spin up electrons occupying the 15 molecular 3*d*–O levels of the isolated $Fe_3O_{14}^{20-}$ sub-unit (Fig. 4a), with the extra spin down electron filling the σ level. It can be noted from Fig. 4 that the distorted cluster is slightly stabilized with regard to the ideal one. This is a direct consequence of the monomer Jahn–Teller effect (see Section 3). In the ideal sub-unit (Fig. 4b), the width of t_{2g} and e_g levels are smaller than the corresponding quantities in the distorted sub-unit (Fig. 4a), consistently with level separation upon distortion. As the 15 spin up electrons completely fill the 3*d* spin up MO levels, a picture which emerges from the present approach is that of a single (spin down) electron moving in a background of $S=5/2$ Fe^{3+} cations.

Differences between the ludwigite and ideal geometries are more stricking in the extended models. In Fig. 5, the band structure and projected DOS curves of the infinite ribbons are shown for both geometries. One could notice first that the effects of distortion are stronger in the t_{2g} bands. When the ideal geometry is considered (Fig. 5a), three t_{2g} wide bands spread across six narrower ones. Whereas, in the actual ludwigite ribbon (Fig. 5b), two bands appear, below and above

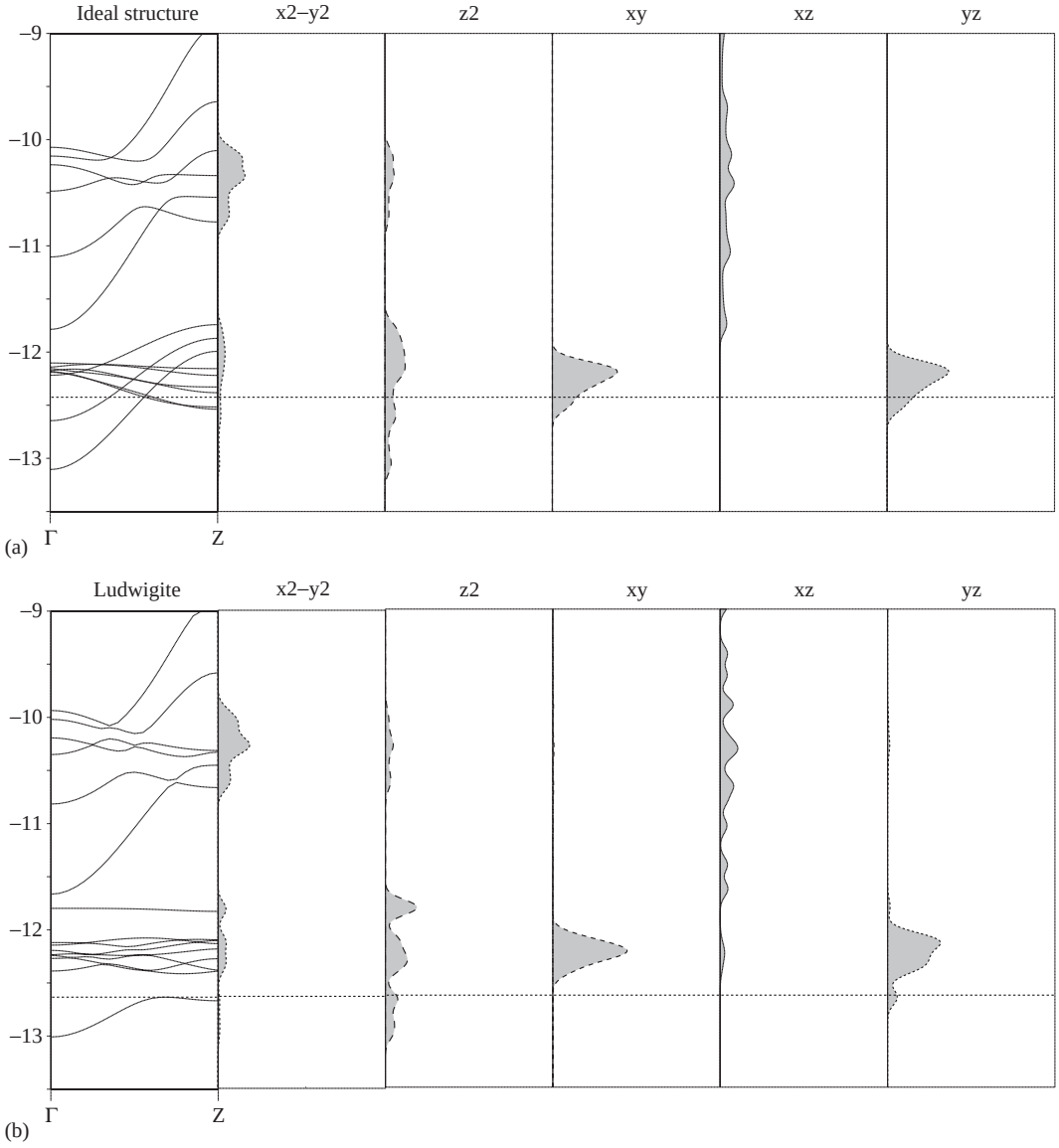

Fig. 5. The band structure and orbital-projected DOS of the ideal (a) and ludwigite (b) ribbons, shown in the energy region of Fe 3d bands. The 9 lower bands come from the t_{2g} group of individual FeO_6. The doted line indicates the spin-down Fermi level. Energies in eV.

the t_{2g} group. These, as seen from the projected DOS curves, originate mainly from z^2 and x^2-y^2 orbitals, with some contribution from yz. As z^2 and x^2-y^2 provide σ bonding (see the coordinate axis in Fig. 3), they will be called σ and σ^* bands [4]; this is in complete analogy with the σ and σ^* levels of the isolated molecular sub-units. e_g bands arise mainly from xz orbitals, as expected, due to the orientation of Fe–O axial bonds (Fig. 3). These bands are in fact mainly due to the triad. This could be seen in a 3D model, eHT calculation, of $Fe_3O_2BO_3$ [4] which shows strong contributions of Fe(2) and Fe(4) in their energy region. In the ideal structure, DOS analysis does not provide the orbital origin of the wide bands due to crossing with the narrow bands. Below, a more detailed analysis will show that they are indeed of the z^2 and x^2-y^2 kind.

To describe high spin configuration in the extended system, the finite system ideas are followed; one then thinks of the 15 spin up electrons per unit cell of $Fe_3O_{10}^{12-}$ as filling the 15 3*d* (spin up) bands, with the extra (spin down) electron occupying the σ band. This defines the *spin-down* Fermi level, at $E_F=-12.63$ eV. The procedure of populating higher lying levels in the extended Hückel theory, devoted in principle to describing the system's ground state configuration, can be justified. In the present case it aims essentially at determining the Fe^{2+} spin down level upon which the analysis is based. Note that the latter quantity stays in the energy region of lower Fe-3*d* levels, that are occupied in the standard (zero spin) ground state configuration of $Fe_3O_2BO_3$.

Above E_F a gap appears with $\Delta E=0.22$ eV and $\Delta k=0.05(\pi/c)$. In the ideal structure, the spin down Fermi level stays at -12.42 eV, inside the t_{2g} band, as seen in Fig. 5a. Such an ideal system would then be conducting, showing oxygen distortion as responsible for the insulating character of the 424 ludwigite chain. For a comparison between Fe and other metal borates it could be remarked that the pentaborate $BaB_5O_8(OH)_3$ is also a semiconductor but in this case the gap is due to O(2p)–B(2p) bonding-antibonding splitting. This leads to much higher energy gaps, of about 5 eV to ~7 eV for different points in the Fermi surface [9].

A more detailed analysis of the effects of distortion on the band structure can be developed if one looks at the actual crystal orbitals. True crystal orbitals ψ_k are formed when the AO combination at a unit cell R, ϕ_R, is summed over the whole crystal according to Bloch's theorem, that is, $\psi_k=\sum_R e^{ikR}\phi_R$. In Fig. 6, the predominant atomic orbitals of ϕ_R are represented at some points. For simplicity, these points will be referred to as A–D for the ideal (Fig. 6a) and A′–D′ (Fig. 6b) for the ludwigite systems, according to their position in the band structure diagram.

In the ideal structure, the ϕ_R are bonding (A and C) and anti-bonding (B and D) combinations of z^2 and x^2-y^2 orbitals with very little contribution of O-p_z (at Γ) and O-p_x (at Z). It was also seen that the intermediate large band that spreads between the former two has anti-bonding combinations of z^2 and x^2-y^2 centered at the two Fe^{3+} (at the triad edges). The character of these orbital combinations reproduces that of a linear arrangement of three H atoms, say, in positions 1, 2 and 3: $\phi_1+\phi_2+\phi_3$; $\phi_1-\phi_3$; $\phi_1-\phi_2+\phi_3$. The six narrower bands of Fig. 6a are H_3-like combinations of xy and yz orbitals. Note the absence of xy, xz and yz orbitals in the ideal wave functions.

For the ludwigite chain (Fig. 6b) one gets the same bonding (A′ and C′) and anti-bonding (B′ and D′) combinations of z^2 and x^2-y^2 orbitals at Γ and Z. In this case, however, as a result of distortion, significant contribution from yz appears at B′ and C′, respectively, 0.15 and 0.67. At A′ and D′, yz contribution is negligible, being both smaller than 0.002. O–2*p* orbitals give also very little contribution (below 0.0004). The wave functions drawn in Fig. 6 show an interesting movement of the bands as one goes from the ideal to the actual ludwigite system. While points A and D practically do not change their position, points B and C "move" up and down under the effect of yz mixing. It can be noticed that the stabilizing interaction at C′ (with 0.67 contribution of yz) is expectedly to be stronger than the destabilizing interaction at B′ (with 0.15 contribution), as it is indeed observed.

The changes observed in the band structure do not depend on the particular choice of the ideal octahedral size, as orbital mixing is determined by symmetry. Through additional calculations it was seen that the general aspect of the ideal ribbon band structure is not affected by small variations of the Fe–O distance. A simple theoretical picture for the formation of the σ and σ^* bands in the ludwigite is that of *squeezing* and mutual repulsion of the upper and lower *ideal* $(z^2)+(x^2-y^2)$ bands through yz mixing, allowed by distortion.

Inter-cell interactions contribute as well to the system's energetics, specially affecting bandwidths [13,16]. The squeezing band mechanism points towards narrower bands in the ludwigite, as compared to the ideal structure. Let us now discuss how do inter-cell interactions affect the particular width of σ and σ^* bands. The aspect taken by ψ_k at each of the four positions in Fig. 6b is sketched in Fig. 7. At A′ and B′ ($k=0$) bonding inter-cell combinations arise, since the crystal wave function coefficients are all unity: $\exp(ikr)=\exp(0)=1$. At C′ and D′, the Bloch coefficient of the *n*th unit cell is given by $\exp[i(\pi/c)nc]=\exp(in\pi)=(-1)^n$, thus leading to inter-cell anti-bonding combinations.

Let us consider interactions involving z^2, x^2-y^2 and yz. These would independently lead to *s*-like bands since the orbitals are symmetric with respect to reflexion in a plane perpendicular to the crystal axis (note that this is

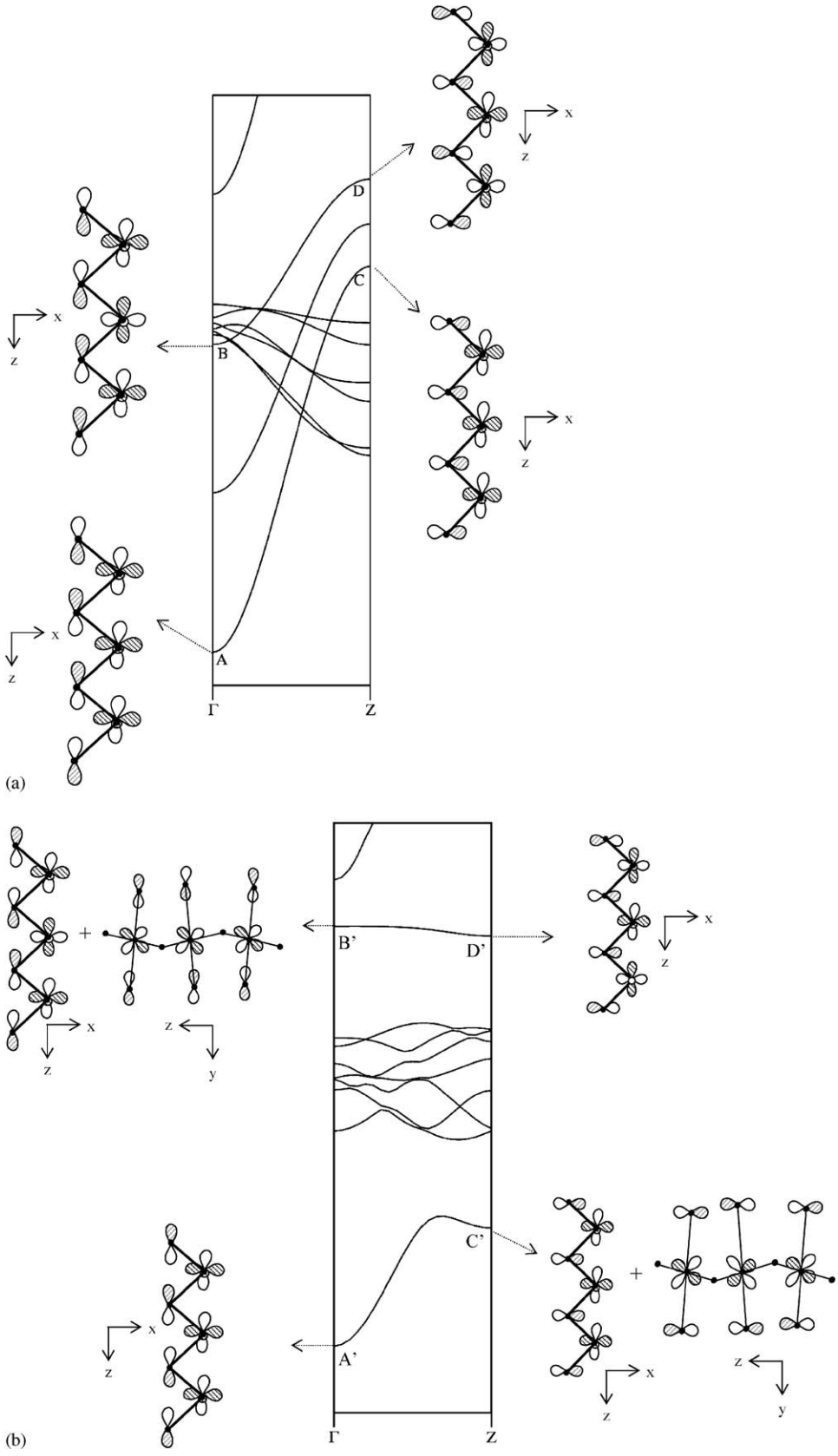

Fig. 6. Representation of the unit cell component (ϕ_R) of the crystal wave functions in four positions, for the ideal (a) and ludwigite (b) ribbons. The wave functions are represented in the coordinate system of Fig. 4.

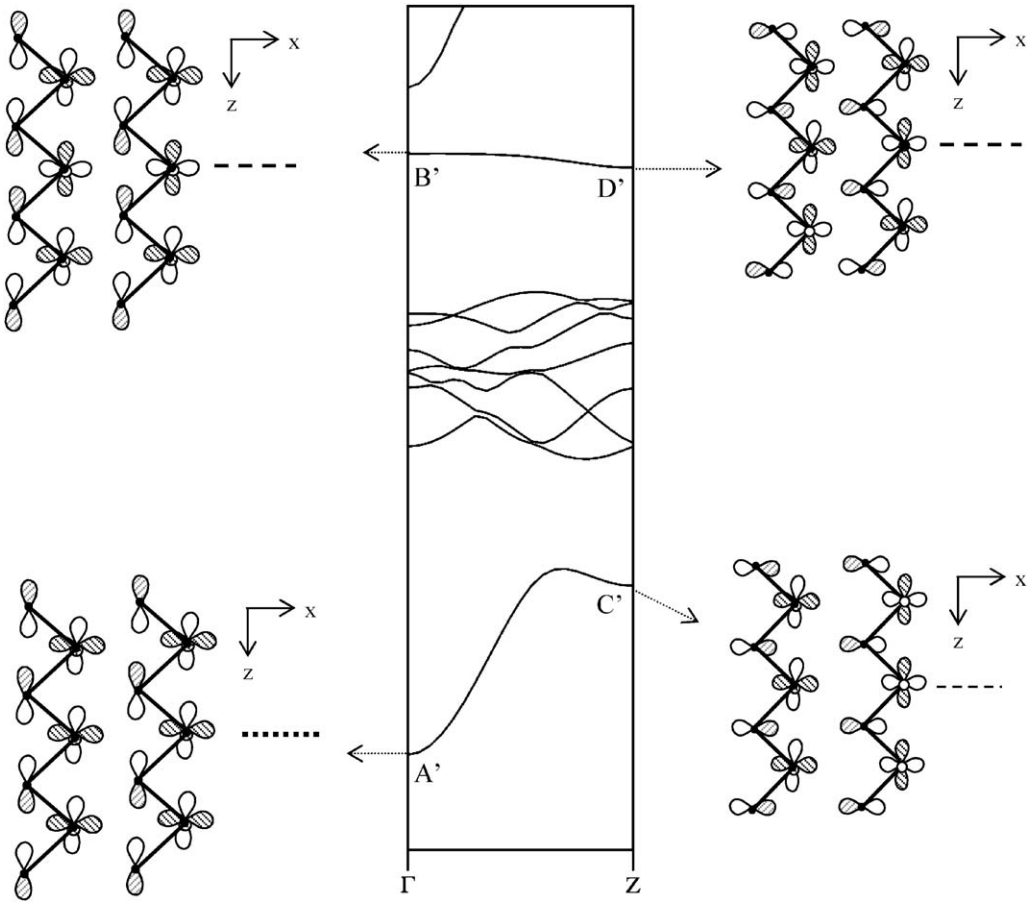

Fig. 7. Representation of the true crystal wave functions (Ψ_k) in the four positions of Fig. 7 for the ludwigite ribbon. Inter-cell bonding combinations (at Γ) are indicated by a repetition of shaded-white lobes of the several orbitals. In the anti-bonding inter-cell combinations (at Z), black and white lobes are interchanged.

Table 2
The character of inter-cell Fe–O interactions in the ludwigite ribbon at the four points (A′–D′) represented in Fig. 7. Fe–O interactions are numbered 1–6, from top to bottom of the wave functions drawn in Fig. 7

From top to bottom	$3d_z^2$–$2p_z$ interactions				$3d_{x2-y2}$–$2p_z$
	$\sigma(\Gamma)$: A′	$\sigma^*(\Gamma)$: B′	$\sigma(Z)$: C′	$\sigma^*(Z)$: D′	$\sigma^*(Z)$: D′
1	Antibonding	Antibonding	Zero contr.	Antibonding	Bonding
2	Bonding	Antibonding	Antibonding	Bonding	Antibonding
3	Antibonding	Antibonding	Antibonding	Antibonding	Bonding
4	Antibonding	Antibonding	Antibonding	Antibonding	Bonding
5	Bonding	Antibonding	Antibonding	Bonding	Antibonding
6	Antibonding	Antibonding	Zero contr.	Antibonding	Bonding
Net result	2-Anti	6-Anti	4-Anti	Cancels out	

also true for yz, not shown in Fig. 7). One could then expect the same behavior for the mutual interaction of the three orbitals. As σ and σ* bands do not present a simple s-like character, one must consider Fe–O interactions. These behave in multiple ways. In Table 2, the nature of several inter-cell Fe–O interactions is given, by considering $2p-z^2$ bonds. In a more quantitative analysis, these should be considered the most important terms, as z^2 provides the strongest contribution to the wave functions (0.27–0.73). At D′, an equivalent contribution from x^2-y^2 is observed (0.39 for total square coefficients in the triad).

It can be noticed from Table 2 that, at B′ and C′, all Fe–O interactions are anti-bonding, differently from A′ and D′. One could expect Fe–O interactions to act so as to increase the energy of C′ more than that of A′, thus

leading to an increase of the σ bandwidth comparatively to that of σ^*. In the latter, the anti-bonding Fe–O contribution at $k=0$ acts energetically so as to oppose the effect of Fe–Fe interactions. Thus, due to Fe–O interactions, the σ^* width expectedly decreases with respect to the case where purely Fe–Fe interactions existed. Inspection of $2p$–yz inter-cell bonds at B′ and C′ shows that all interactions are anti-bonding, repeating the pattern shown for the other orbitals. Although qualitative, these arguments provide sufficient support to the idea that Fe–O interactions play an important role in determining the particular shapes of σ and σ^*.

Some comments could be made about the intermediate (large width) $z^2+(x^2-y^2)$ band of the ideal structure (Fig. 6a). The effects of distortion are much more complicating to analyze in this case. As seen above, the band arises from anti-bonding combinations of Fe^{3+} orbitals. Through inspection, two crystal wave functions could be identified in the ludwigite ribbon, one at Γ, right above A′, the other one at Z, right below D′, wherein *bonding* Fe^{3+} yz combination are present. These tend to decrease the energy of the band states, both at Γ and Z. At Z the effect is clearly to bring the large intermediate band of the ideal structure close to the narrower bands. At Γ, the effect is not clear; however it is reasonable to expect that other (e.g., Fe–O) interactions could act so as to compensate the bonding mixture of yz, thus pushing the band upward. Both effects expectedly lead to the squeezing of the ideal intermediate band, analogously to the other two.

It is interesting to discuss Mulliken population. Qualitatively different results are obtained when high and low spin band approaches are used. In the former, calculations give the quantities 1.255 and 1.473, respectively, for Fe(2) and Fe(4) total Fe charges in the ludwigite ribbon. The fact that Fe(2) has lower charge than Fe(4) is consistent with the expected tendency of Fe(4) and Fe(2) to have formal charge +3 and near +2, respectively, as seen from the bond valence estimates. When low spin configuration is considered (in which the crystal levels are filled according to the Aufbau principle), a reversal of charge distribution is obtained, with the quantities 1.544 and 1.050 associated to Fe(2) and Fe(4), respectively. Such a reversal was discussed in a previous study of the ludwigite [4]. Similar results are obtained in the ideal geometry, in which one gets for Fe charges in high(low) spin, 1.198(1.166) and 1.307(1.094), respectively, for Fe(2) and Fe(4).

Electron transfer from Fe to O occurs preferentially in the axial direction whose anions have charge −1.763 and −1.780/−1.776 respectively at central and external (left or right) axial positions, being the more highly charged O atom nearer to the central axial oxygen (top left O axial atom in Fig. 3). On the other hand, bridging anions have charge −1.274 (O central atoms) and −1.510 (O external atoms). Such oxygen electron distribution is similar to that in the ideal structure where axial anions have charges −1.774 (central) and −1.776 (external), while bridging anions bear −1.219 (central) and −1.590 (external) charges.

Average COOPs were calculated for the interaction between Fe and equatorial as well as axial oxygens. The obtained results are 0.16 for $Fe–O_{eq}$ and 0.20 for $Fe–O_{axial}$, consistently with the observed Fe to O charge transfer, discussed above. These values indicate stronger interaction with axial than with equatorial oxygens. Even though a quantitative comparison with the ideal structure should not be considered conclusive, it could be mentioned that within the present choice of Fe–O distance, the average COOPs turn out to be *smaller* in the ideal structure, being 0.09 and 0.11 for equatorial and axial Fe–O interactions, respectively. This would indicate an increase in Fe–O interactions through distortion.

Charge distribution in the ludwigite ribbon was compared with that obtained with two other model systems, namely a 2D sub-unit, describing an isolated zig-zag wall, and the full 3D crystalline structure. Results are given in Table 3, both for high and low spin configurations. In the low spin case, no significant differences are noticed when one goes from the 3D to the 1D models. However, within the high spin band model, significantly different oxidation states are obtained only within the ribbon. In the 3D system, electrons delocalize across the four crystallographic sites, giving rise to an equalization of Fe charge among all sites, most likely due to inter-triad and inter-wall interactions. Note that an extra path exists in the 3D structure, not present in the 2D sub-unit. In the latter, some localization still remains, with electrons flowing to Fe(2). As delocalization is manifested only within the high spin model, in which different spins have different spacial distribution, these results indicate that interactions involving the spin down electrons of Fe^{2+} are responsible for charge delocalization in $Fe_3O_2BO_3$. Note that spin up electrons completely fill the $3d$ spin up levels, having, consequently, low mobility. The present inter-wall charge delocalization effect is

Table 3
Total Fe charges, in atomic units, at the four crystallographic sites of $Fe_3O_2BO_3$ for the 3D (whole crystal), 2D (zig-zag wall) and 1D (ribbon) models

	High spin			Low spin		
	3D	2D	1D	3D	2D	1D
Fe(1)	1.004	0.940	—	0.633	0.682	—
Fe(2)	1.234	1.126	1.255	1.509	1.516	1.544
Fe(3)	1.198	1.265	—	0.664	0.669	—
Fe(4)	1.235	1.215	1.473	0.959	1.029	1.050

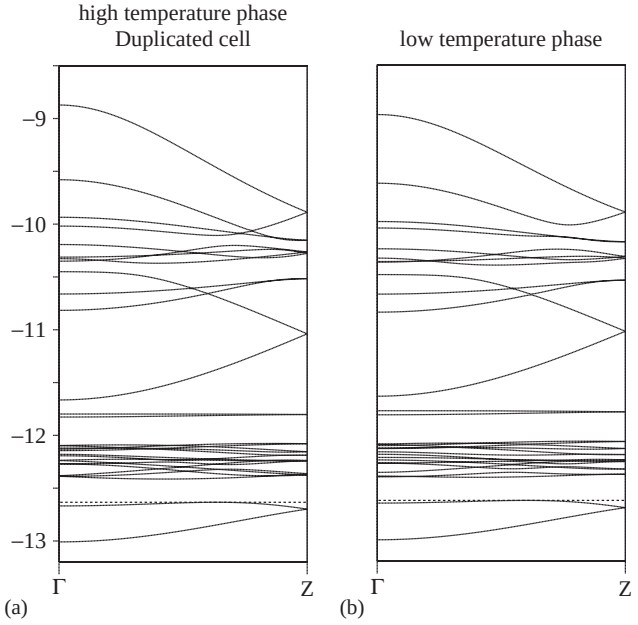

Fig. 8. The band structure of the 1D sub-units of two crystalline phases of $Fe_3O_2BO_3$ showing the Fe–3*d* bands: (a) the high temperature, high symmetry phase; (b) the low temperature, low symmetry phase. The Fermi level, shown in broken lines is −12. 63 and −12.62 eV in (a) and (b), respectively. Energies in eV. In (a), the unit cell was duplicated to allow comparison with (b).

consistent with the Fe(1)–Fe(3) spin exchange path found in Ref. [5].

The above results were based on the high temperature crystalline phase of the Fe ludwigite, of higher symmetry with regard to the low temperature phase. In Fig. 8, the electronic band structure of the 1D sub unit of the two phases is shown for comparison. For the high-temperature phase (Fig. 8a), the unit cell was duplicated to allow comparison with the less symmetric phase (Fig. 8b). It can be noted that distortions, which reduce the symmetry at low temperatures do not affect significantly the electronic band structure of the material. In particular, the t_{2g} band, upon which the analysis was based, remains practically unchanged. The gap above the spin down level is indeed found to be 0.22 eV, the same as that obtained in the high-temperature phase. Thus, the arguments presented in this section, based on the existence of the 1D gap, can be applied to both crystalline phases of the material. Owing to the strong similarity of the Fe–3*d* band structure of both phases, it is also reasonable to expect that the theoretical analysis developed above could be used with no fundamental changes in the less symmetric phase of $Fe_3O_2BO_3$.

5. Discussion

The existence of an electronic barrier in $Fe_3O_2BO_3$, associated to charge localization and high resistivity at lower temperatures, has been already suggested [1,2]. In particular, Swinnea et al. [1], point out that the short Fe(2)–Fe(4) (2.787 Å) distance in the triad cluster, as opposed to the longer Fe(2)–Fe(2) and Fe(4)–Fe(4) distances along c (3.075 Å), could explain the experimental evidence that intermediate valence +2.5 be found in the compound, besides 3+ and 2+. According to this picture, electronic transport along the 424 chain would be the mechanism responsible for charge delocalization at higher temperatures.

The present theoretical analysis has shown that the 1D Fe(4)–Fe(2)–Fe(4) sub-unit behaves as a small gap semiconductor. If one accepts that electronic conductivity along the 424 stripe is relevant to the transport behavior of the material, as suggested above, the 1D gap could be seen as the electronic origin for the barrier believed to exist in the material. In a previous study [4] it was shown that for the whole crystal the σ band overlaps with higher energy t_{2g} bands; in addition, the spin down Fermi level is pushed up, due to the presence of other divalent cations, Fe(1) and Fe(3). Thus, the gap disappears as a result of inter-wall interactions. In a more complete picture, the conductivity of $Fe_3O_2BO_3$ could be seen to be related to electronic paths connected to Fe(1) and Fe(3) divalent cations at lower temperatures and being raised by $Fe(2)^{2+}$ electrons overcoming the 1D 424 gap at higher temperatures.

Another indication of the role of inter-wall interactions in the electronic processes discussed in this paper is provided by the calculated 3D Fe charge distribution, which indicate delocalization. This is consistent with the band structure prediction of 3D transport. On the other hand, in a more localized point of view, if the barrier for electron hopping along the triad is associated to an Fe–Fe distance of 3.075 Å, it is reasonable to assume that other barriers exist, since there are several Fe–Fe distances in the material close to *c*. This would explain high resistivity at lower temperatures, besides the existence of 3D paths for conduction. The understanding of the exact electronic mechanism in a 3D transport would require more investigation. However, the present study provides a basic theoretical picture of important electronic mechanisms present in this complex compound.

6. Conclusion

In this paper, the high spin band approach was applied to the extended Hückel approximation, to investigate structural effects in the electronic properties of the magnetic homometallic Fe ludwigite. A detailed analysis was performed by comparing a 1D sub-unit of the ludwigite, made of the 424 Fe triad running along the *c*-axis, with an ideal equivalent.

It was shown that distortions of the octahedral field, present in the ludwigite, are responsible for the appearance of a stabilizing gap of 0.22 eV above the spin down Fermi level. More specifically, the gap is due to mixing of z^2 and x^2-y^2 with yz $3d$ orbitals, being allowed by symmetry lowering with regard to the ideal octahedral geometry. It is suggested that the 424 triad gap is related to the barrier for electrical conductivity in the system, already suggested in the literature.

Charge distribution was also investigated. It was found that localization appears in the 1D chain when high spin configuration is used. In the whole 3D crystal, Fe charges are more delocalized due to inter-wall interactions. Since in the usual low spin configuration (Aufbau principle) no significant differences are noted in the charge distribution of 1D and 3D models, it is suggested that delocalization is related to inter-wall interactions involving the extra, spin down, electrons of the divalent Fe^{2+} cations. It is also suggested that the temperature dependence of the electrical conductivity could be understood as a result of different paths connected to the several Fe^{2+} cations in $Fe_3O_2BO_3$.

The present results show that the extended Hückel high spin band approximation gives a better description of some basic physical properties of $Fe_3O_2BO_3$ than the more usual ground state, low spin configuration. In particular, while the latter leads to a reversal in the crystalline positions of Fe^{2+} and Fe^{3+}, the calculated charge distribution within the high spin band approach is consistent with experimental evidence of metal oxidation state distribution in $Fe_3O_2BO_3$. A complete explanation of the material's electronic structure would require more sophisticate ab initio theoretical calculations, which properly took into account spin polarization and electron–electron interaction effects. The present analysis, providing simple understanding of basic electronic processes in the structure–property relationship, could help any future theoretical investigations in this material.

Acknowledgments

All extended Hückel calculations have been performed by using the yaehmop package, developed by Dr. Greg Landrum.

References

[1] J.S. Swinnea, H. Steinfink, Am. Mineral. 68 (1983) 827–832.
[2] R.B. Guimarães, M. Mir, J.C. Fernandes, M.A. Continentino, H.A. Borges, G. Cernicchiaro, M.B. Fontes, D.R.S. Canela, E. Baggio-Saitovitch, Phys. Rev. 60 (1999) 6617–6622.
[3] J.C. Fernandes, R.B. Guimarães, M.A. Continentino, L. Ghivelder, R.S. Freitas, Phys. Rev. B 61 (2) (2000) R850–R854.
[4] M. Matos, E.V. Anda, J.C. Fernandes, R.B. Guimarães, J. Mol. Struct. (Theochem) 539 (2001) 181–190 (see Fig. 4 of this reference for the monomer degeneracies, cited in this text).
[5] M.-H. Whangbo, H.-J. Koo, J. Dumas, M.A. Continentino, Inorg. Chem. 41 (2002) 2193–2201.
[6] M. Mir, R.B. Guimarães, J.C. Fernandes, M.A. Continentino, A.C. Dorigueto, Y.P. Mascarenhas, J. Ellena, E.E. Castellano, R.S. Freitas, L. Ghivelder, Phys. Rev. Lett. 87 (14) (2001) 146201–147204.
[7] R. Norrestam, M. Kritikos, K. Nielsen, I. S¢tofte, N. Thorup, J. Sol. State Chem. 111 (1994) 217–223. (For a discussion on the structures of ludwigites and warwickites, see Y. Takéuchi, Takéo Watanabe, T. Ito, Acta Crystallogr. 3 (1950) 98–107.
[8] M. Matos, R. Hoffmann, A. Latgé, E.V. Anda, Chem. Mater. 8 (9) (1996) 2324–2330.
[9] P. Smok, I.V. Kityk, K.J. Plucinski, J. Berdowski, Phys. Rev. B 65 (2002) 205103(1-6).
[10] R. Hoffmann, J. Chem. Phys. 39 (1963) 1367–1412.
[11] M.-H. Whangbo, R. Hoffmann, J. Am. Chem. Soc. 100 (1978) 6093–6098.
[12] J.H. Ammeter, H.-B. Bürgi, J.C. Thibeau, R. Hoffmann, J. Am. Chem. Soc. 100 (12) (1978) 3686–3692.
[13] R. Hoffmann, Solids and Surfaces, VCH, 1988.
[14] I.D. Brown, D. Altermatt, Acta. Crystallogr., B 41 (1985) 244–247.
[15] S. Shaik, R. Hoffmann, C.R. Fisel, R.H. Summerville, J. Am. Chem. Soc. 102 (1980) 4555–4572.
[16] M.-H. Whangbo, in: J. Rouxel (Ed.), Crystal Chemistry and Properties of Materials and Quasi-One-Dimensional Structures, D. Reidel Publ. Co., 1986, pp. 27–85.